Microbiological and decomposition analysis of mass mink burial sites during the COVID-19 pandemic

Thamsborg, Kristian Key Milan; Hansen, Mette Sif; Scheutz, Charlotte; Klintø, Kasper; Kjeldsen, Peter; Kvisgaard, Lise Kirstine; Jensen, Henrik Elvang; Hjerpe, Freja Broe; Lohse, Louise; Rasmussen, Thomas Bruun

Total number of authors:
15

Published in:
Scientific Reports

Link to article, DOI:
10.1038/s41598-024-69902-6

Publication date:
2024

Document Version
Publisher's PDF, also known as Version of record

scientific reports

Check for updates

OPEN

Microbiological and decomposition analysis of mass mink burial sites during the COVID-19 pandemic

Kristian Key Milan Thamsborg[1], Mette Sif Hansen[1], Charlotte Scheutz[2], Kasper Klintø[3], Peter Kjeldsen[2], Lise Kirstine Kvisgaard[1], Henrik Elvang Jensen[1], Freja Broe Hjerpe[4], Louise Lohse[4], Thomas Bruun Rasmussen[4], Lasse Dam Rasmussen[4], Amalie Ehlers Bedsted[1], Graham J. Belsham[1], Jørgen J. Leisner[1] & Anders Dalsgaard[1]✉

In 2020, Denmark buried approximately four million culled, farmed mink in mass graves treated with slaked lime due to widespread SARS-CoV-2 infections. After six months, environmental concerns prompted the exhumation of these cadavers. Our analysis encompassed visual inspections, soil pH measurements, and gas emission assessments of the grave environment. Additionally, we evaluated carcasses for decay status, cadaverine content, and the presence of various pathogens, including SARS-CoV-2 and mink coronavirus. Our findings revealed minimal microbial activity and limited carcass decomposition. Although viral RNA from SARS-CoV-2 and mink coronavirus, along with DNA from Aleutian mink disease virus, were detected, the absence of infectious SARS-CoV-2 in cell culture assays suggests slow natural degradation processes. This study provides critical insights for future considerations in managing mass burial scenarios during outbreaks of livestock-associated zoonotic pathogens.

SARS-CoV-2 spread rapidly within and between Danish mink farms from June to November 2020, infecting 290 farms, which included 25% of all Danish mink farms[1,2]. On multiple occasions, the virus was transmitted from humans to mink and from mink to humans on these farms, leading to subsequent community spread of mink-associated SARS-CoV-2 strains[1,3]. On November 4th, 2020, the Danish government announced that all mink in the country, approximately 17 million animals, were to be euthanized and securely disposed of to eliminate the risk of new virus variants evolving in the mink and further transmission of SARS-CoV-2 to the human population[1]. As part of a large culling process and due to limited incineration capacity, approximately four million mink were buried at two sites in Jutland, Denmark. However, subsequent environmental concerns, primarily regarding the risk of groundwater contamination at the burial sites, led authorities to decide that the mink should be exhumed after six months, when the carcasses were expected to no longer pose any infectious risks. The exhumed carcasses were then disposed of by incineration.

Carcasses buried in soil typically decompose more slowly compared to those submerged in water or exposed to air[4,5]. A key factor determining the rate of decay is how quickly the carcasses are buried after death. If the decomposition processes are less advanced at the time of burial, the post-burial decomposition will proceed more slowly. Conversely, if decay processes have already started by the time of burial, these processes will continue, albeit at a reduced rate, potentially leading to tissue liquefaction—a phenomenon often observed in unburied carcasses[5]. Low temperature, anaerobic conditions, and limited access by scavengers, rodents, and insects tend to preserve the carcass[5,6]. Soil type also impacts decay; highly permeable sandy soils allow atmospheric air and rainfall to infiltrate the carcasses, accelerating decay processes, while clay soils, with low permeability, partially or completely prevent the passage of air and water[5]. Due to these varying factors, it is challenging to establish a universal timeline for the decay processes in buried carcasses.

A shift in the bacterial community from aerobic to anaerobic microorganisms can be expected during the decomposition of animal carcasses[7]. Intestinal bacteria, particularly clostridia, constitute the main component of the carcass microbiota[8]. The use of disinfectants is important when large volumes of dead animals are buried, but

[1]Department of Veterinary and Animal Sciences, University of Copenhagen, Grønnegårdsvej 15, 1870 Frederiksberg C., Denmark. [2]Department of Environmental and Resource Engineering, Technical University of Denmark, Bygningstorvet, Building 115, 2800 Kgs, Lyngby, Denmark. [3]Danish Veterinary and Food Administration, Stationsparken 31-33, 2600 Glostrup, Denmark. [4]Department of Virus and Microbiological Special Diagnostics, Statens Serum Institut, Artillerivej 5, 2300 Copenhagen, Denmark. ✉email: adal@sund.ku.dk

it can slow down carcass decomposition. The disinfection effect of slaked lime on microbial activity[9], including the formation of microbial metabolites such as methane (CH_4), hydrogen sulfide (H_2S), nitrous oxide (N_2O), and ammonia (NH_3), depends on the distribution of lime around the carcasses and the pre-burial condition of the carcasses, such as the integrity of the skin, bloating, and the stage of decomposition.

Large outbreaks of infectious livestock diseases are ongoing and are likely to occur in the future. For example, African swine fever and avian influenza are immediate threats, with the former recently causing devastating outbreaks in the pig sectors of China, Vietnam, and several European countries[10–12]. Recently, outbreaks of highly pathogenic avian influenza (H5N1) in poultry and multiple mammalian species have been reported in Europe and the United States[13,14]. The outbreaks of SARS-CoV-2 infection in Danish mink farms in 2020 have highlighted the importance of being prepared and having effective contingency plans for safely handling and disposing of large quantities of potentially infectious carcasses. Such procedures often include the burial of culled livestock due to the limited capacity of incineration plants to process large numbers of carcasses in a short time.

The current study provided a unique opportunity to gain knowledge on the decay status, microbiological, and environmental features of mink culled due to the SARS-CoV-2 pandemic, as the carcasses were exhumed after six months from graves with added slaked lime. Our findings and experiences can aid in future planning for the rapid disposal of large quantities of dead livestock, thereby preventing the spread of animal or zoonotic infectious agents.

Results

Characteristics of the mink graves

The mink graves were located at two sites near the small towns of Nørre (Nr.) Felding (near Holstebro) and Kølvrå (near Karup). These locations are hereafter referred to as the Holstebro and Karup sites, respectively. At the Holstebro site, graves were 3 m wide and constructed in 16 segments with a total length of 1810 m. At the Karup site, grave segments had a width between 3 and 4 m and a total length of 1623 m. Six graves (G1-G6) were selected from these segments for the detailed analyses reported in this study (Fig. 1A,B). The graves were established at the Karup site from November 7th to 27th, 2020, and at the Holstebro site from November 8th to 20th, 2020. Excavation and sampling, except for gas analyses, were performed from May 25th to 31st, 2021, at the Holstebro site and from June 19th to 28th, 2021, at the Karup site. On-site gas analyses were conducted before excavation on May 5th, 2021, at the Karup site and from May 20th to 21st, 2021, at the Holstebro site.

The soil in the graves beneath the carcass mass and the slaked lime layers was composed of geologically original compact substratum. In contrast the soil above the mink and slaked lime layers had been excavated during the process of positioning of the carcass mass. Subsequent the soil was repositioned as the cover soil, in a noncompact mixed porous manner.

During the initial burial process, it was observed that the mink layer became displaced in the graves when the soil was added on top of the mink carcasses, as described below. To prevent this displacement, soil was subsequently deposited in successive layers above the graves at both disposal sites. Additionally, at the Karup site, vertical soil barriers, approximately one meter in height, were placed at 30-m intervals within each grave to prevent longitudinal movement of the mink layer (Fig. 1C).

During the burial procedure, slaked lime was continuously added on top of the mink layer before soil was added. Over a period of three weeks after burial at the Holstebro site, several displacements and surface eruptions of mink carcasses occurred, each lasting for two to three days (Fig. 1D). These eruptions occurred gradually, with the carcasses showing signs of putrefaction, such as foul odor, skin discoloration, and bloating. Once the eruptions settled, the surfaced carcasses were removed and re-deposited in an additional segment at the gravesite. This type of surface eruption was not observed at the Karup site.

At both disposal sites, different types of displacements were observed in the soil above the mink layer. Both sinking and elevation of the soil surface were common. At the Karup site, the soil in the center of the graves subsided, while the soil along the edges and above the ridges was elevated. At some graves at both the Karup and Holstebro sites, fluids and putrefied sulfurous gases were continuously released from cracks and eruption spots in the soil for three weeks post-burial. Visible eruption formations (Fig. 1E) of solidified fluid from the carcasses with lime content occurred when re-deposited. In multiple locations at both disposal sites, minor eruptions of small plate-like structures originated from crevices in the soil surface (Fig. 1E).

When the mink were exhumed six months post-burial, the soil above the graves appeared uniform, with no visible traces of the added slaked lime. However, significant differences in the amount of soil located above the mink layers were observed at the Holstebro site. Upon excavation, the first layer of slaked lime was often associated with a puddle of water above it in nearly all examined graves. The slaked lime itself appeared as a white or green/bluish material (when wet) mixed with the soil both above and beneath the mink layer at all sampling spots.

The mink carcasses were generally found in uneven layers, with the height of these layers varying from 0.5 to 2 m in several of the graves at the Holstebro site. In contrast, carcasses were displaced to the sides of several graves at the Karup site. The outermost mink carcasses were frequently covered in slaked lime on the side facing upwards, leaving the other side and the rest of the mink unexposed to the slaked lime. No accumulation of water was observed at the bottom of the graves. The soil surface of the graves had often sunk to different heights of 0.2 to 1 m at both gravesites. The sinking and rising of the ground surface were most likely caused by a combination of the natural settlement of the soil cover and the decomposition of the mink carcasses.

Values of pH for graves G1-G6 (Fig. 1A,B) showed considerable variation indicating an uneven distribution of the alkalinity provided by the slaked lime (Suppl. data 1). However, high pH levels were measured for sample G6 (Suppl. data 1) containing visible slaked lime. In summary, the pH values for the graves varied from 5.9 to 12.6 but were generally in the alkaline range (Suppl. data 1).

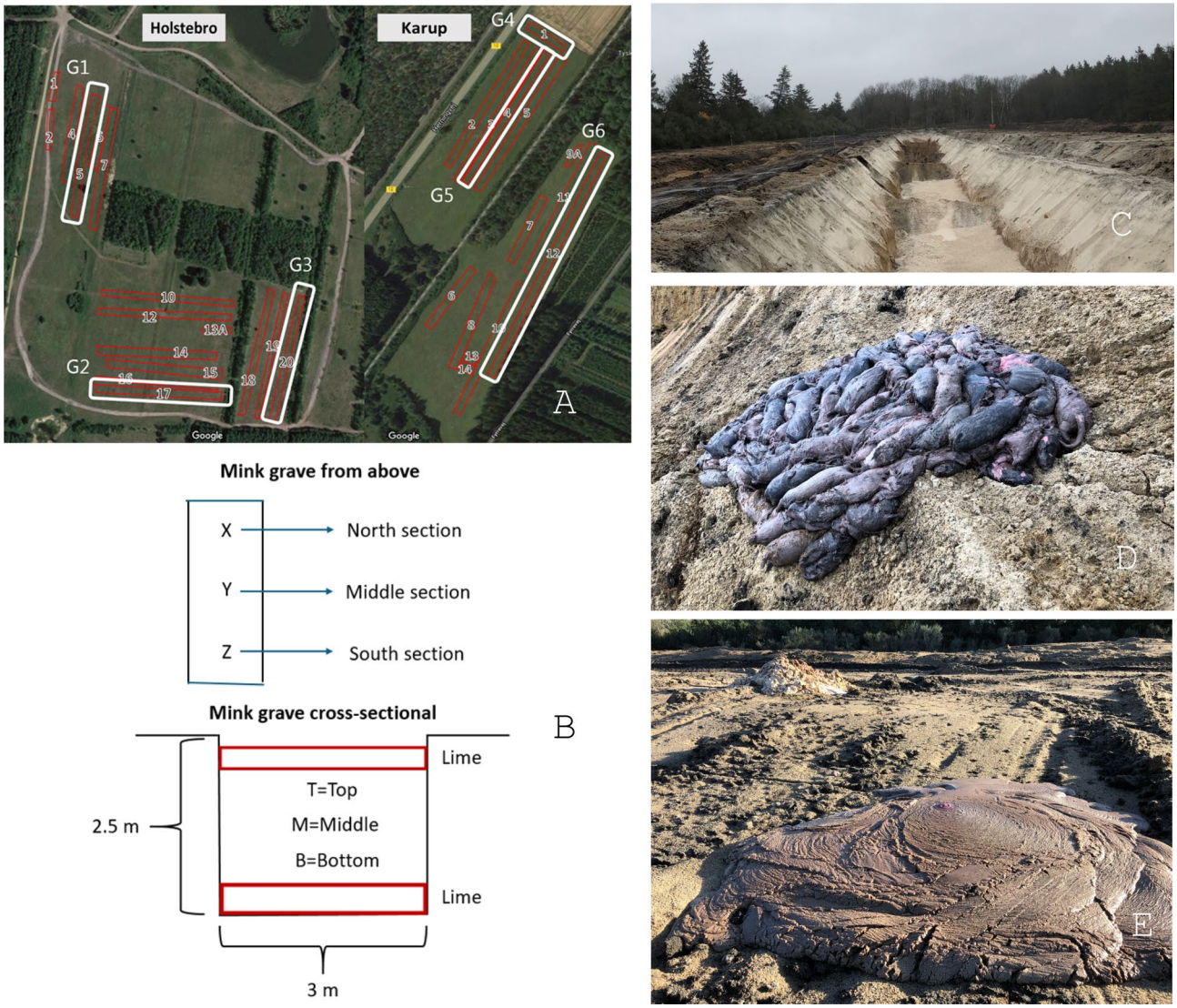

Figure 1. (**A**) Map of Holstebro and Karup disposal sites with selected graves marked with white borders and sampling numbers (G1-G6). See Supplementary file 3 for the location of gas measurement points (Image ©2021 Google, Maxar Technologies). (**B**) Illustration of sampling locations and nomenclature. The illustration on the top is a grave seen from the air, and the illustration in the bottom is a cross-sectional view of a grave. (**C**) Grave with ridges every 30 m to prevent longitudinal displacement of the mink layer (Karup site). (**D**) Displacement and surface eruption of mink carcasses at grave 20 (G3)(Holstebro site). (**E**) An active plate-like eruption. An inactive (dormant) eruption is seen in the background (Karup site).

Microbial levels in the soil at the top and bottom of the graves were examined for one randomly selected grave at the Holstebro site (grave 1, Fig. 1A). Both aerobic and anaerobic bacterial counts in the samples ranged from less than or around $\log_{10}$ 2 to $\log_{10}$ 5.3 colony forming units (CFU)/g of soil (Suppl. data 2). Counts of presumptive clostridia, based on their typical morphology on iron sulfite agar, ranged from between 20 and 2000 cfu/g whereas levels of presumptive clostridial spores in all cases were below 10 cfu/g.

Gas generation and emissions

Despite the displacement and elongated cracks and fissures in the soil cover, surface CH_4 concentration screenings showed very low CH_4 concentrations (2.0–2.5 ppm), which is close to the atmospheric background, indicating minimal CH_4 emission from the mink graves (Suppl. data 3.1). This was confirmed by performing upwind and downwind CH_4 screening with highly sensitive instrumentation showing concentrations comparable to atmospheric background levels. Only a few areas or hotspots on the graves were identified with slightly elevated CH_4 concentrations (up to 4 ppm) (Suppl. datas 3.2–3.3).

Gas concentration profiles in the soil cover showed elevated CO_2 concentrations and reduced O_2 concentrations, especially in the deeper part of the cover. However, only small concentrations of CH_4 (< 40 ppm-level) were measured, and gas concentrations profiles indicated CH_4 oxidation in the shallow part of the cover soil (Suppl. datas 3.4–3.5). During the gas profile measurements, water was often found at 120–160 cm depth, indicating

accumulation of infiltrating water potentially in, or above, the layer of slaked lime added on top of the mink carcasses.

In general, surface emission fluxes of CH_4, CO_2, N_2O and NH_3, measured using static chambers, were very low or below the detection limit even at the few hotspots identified based on surface concentration screening. CH_4 emission fluxes were within the range of -0.001 to 0.035 g m^{-2} d^{-1} with negative fluxes indicating uptake of atmospheric CH_4 by the cover soil. CO_2 emission surface fluxes ranged from below the detection limit to 128 g m^{-2} d^{-1} and were in general elevated in comparison to CH_4 fluxes and compared to background CO_2 fluxes measured outside the graves (Suppl. data 3.6). The elevated CO_2 emission fluxes likely resulted from decomposition of carcasses as well as oxidation of CH_4 in cover soil and were supported by gas concentration profiles.

Overall, the gas investigations showed surprisingly little gas generation from the buried mink cadavers and no significant emissions into the environment from the mink graves. Gas formation mainly consisted of CO_2 with only trace formation of CH_4, H_2S, NH_3 and N_2O. The addition of slaked lime most likely prevented microbial decomposition and preserved the mink during the six-month period after disposal.

Carcass decomposition

At the burial sites, three to five mink were collected from each sampling location in the graves (including top, middle, and bottom levels; n = 54) and stored in plastic boxes, with each box representing one study unit. The 44 boxes with mink carcasses that tested negative in the SARS-CoV-2 PCR test (see materials and methods) were examined macroscopically. These boxes contained either three (n = 37) or five mink carcasses (n = 7), and fluid was not present in any of the boxes. Among the 146 carcasses examined, the surface of the organs within the thoracic and/or abdominal cavity appeared moist in 48 cases. However, the parenchyma of the organs appeared dry in the majority (97%, 142/146) of the mink. A few milliliters of fluid were found within the thoracic cavity of two mink (Fig. 2A,B).

More than half of the carcasses were essentially intact (58%, 85/146; Fig. 3A,C,E), with the most prevalent injuries being the absence of the head and/or openings into the body cavities. No insects were present on or within the carcasses. The body form of the carcasses varied, ranging from flattened to displaying varying degrees of bloating. The internal organs of the bloated mink tended to be moister in the thoracic and abdominal cavities compared to the mink with a flatter body form. In many carcasses, the color of the internal organs appeared pink/red upon opening of the body cavities, but quickly turned brown/grey due to oxidation (Fig. 2C,D). In general, the skin was of almost normal thickness and strength. The fur was, with one exception, always present, though it occasionally detached from the skin when the carcass was manipulated. The head region tended to be the body part where the decay was most advanced, with high decay scores on the skin and ligaments. The

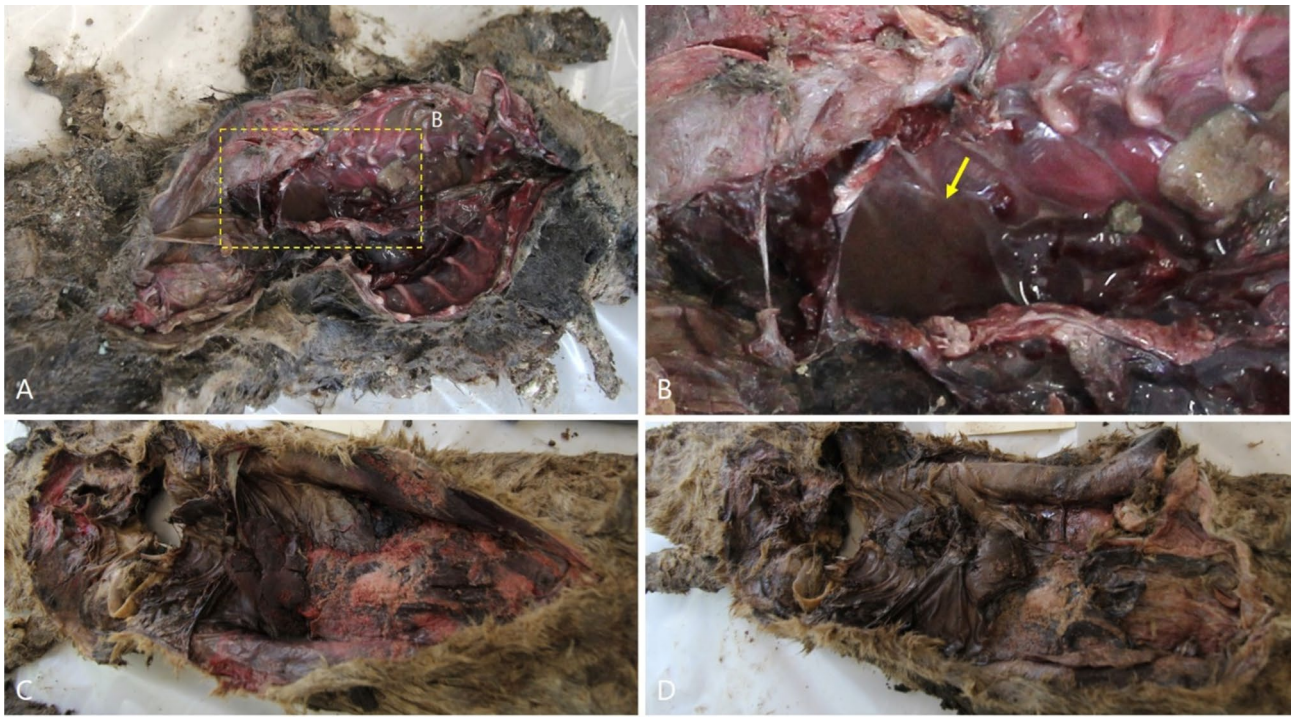

Figure 2. (**A**–**D**) Transparent fluid in the thoracic cavity of one mink from study unit G5-YM, Bradford score = 74. (**A**) Carcass with open thoracic and abdominal cavity. The yellow box represents panel B; (**B**) Detail of panel A with close-up of the fluid in thorax (yellow arrow). (**C**-**D**) Oxidation of a mink carcass from study unit G3-XM, Bradford score = 44. (**C**) Carcass just opened revealing pink/red organs; (**D**) Appearance of the same carcass 12 min after opening, where the color of the organs has turned brown/grey.

Figure 3. Examples of Bradford (BF) scores showing intact mink (**A**, **C**, **E**) and opened carcasses (**B**, **D**, **F**). (**A**) and (**B**) illustrates low Bradford score (Box ID: G5-YM, BF score = 37). Abdominal cavity with "grainy pearls of fat" (yellow arrow); (**C**) and (**D**) Carcasses with average Bradford score (Box ID: G1-XT, BF score = 64). Thoracic cavity with highly decomposed lung and heart tissue (yellow arrow); (**E**) and (**F**) Carcasses with high Bradford score (Box ID: G4-ZT, BF score = 85).

organs in the thoracic cavity (lung and heart) were generally more decomposed compared to the organs in the abdominal cavity (Fig. 3B,D).

The subcutaneous adipose tissue on the torso and extremities (not evaluated on the head) was often not detectable macroscopically. The skeletal muscles on all body parts were frequently decomposed with a creamy, pasty consistency. Almost all ligaments around the jaw joints and joints of the extremities had lost all or part of their tensile strength due to decomposition. In contrast, the periodontal ligaments were well-preserved in most mink. In the abdominal cavity, the stomach was seldom recognizable, whereas the intestines were often identifiable. The structure of the abdominal or subcutaneous fat had changed into "grainy pearls of fat" in 18 (12%) and 3 cases (2%), respectively (Fig. 3B).

The total soft tissue degradation Bradford score (BF, see materials and methods, see Fig. 3A–F for examples) of the head, torso, and extremities in the individual mink in each of the 44 study units showed no correlation with the location of the carcasses in the graves (Suppl. data 4).

The study units were divided into three degradation categories based on their total BF soft tissue scores. In 13/44 boxes (~30%), a degradation category of one (limited changes) was estimated. Seven of these boxes contained carcasses from the middle of the graves out of a total of 14 examined boxes originating from this location. The remaining four boxes with carcasses collected from the middle location in the graves were not examined due to positive SARS-CoV-2 RT-qPCR results. Most of the boxes (~63%; n = 28) had a degradation category score of two, and three boxes (~7%) had a score of three (extensive changes) (Table 1).

From each mink carcass, a block of skin with subcutaneous adipose tissue and underlying muscle was sampled for histology. After formalin fixation, the subcutaneous adipose tissue in the skin blocks was often easily recognizable, however, it appeared gelatinous. Histological examination of the skin blocks showed that the tissue structures were well-preserved with clear distinction between the epidermis, dermis with hair follicles, subcutis, and skeletal muscle (Fig. 4A). However, all nuclei were absent, and it was not possible to identify the outline of the individual cells, except for adipocytes and skeletal muscle fibers. Compared to connective tissue and the epidermis, the muscle fibers more often showed signs of degradation. However, in some samples, the muscle fibers were almost intact with clear striation, whereas in other samples, there was a mix of pieces of intact muscle fibers surrounded by remains of degraded muscle, and finally, in some samples, almost all fibers were completely decomposed (Fig. 4 B, C). Varying degrees of mineralization were present in all tissues, but mainly in the subcutis.

In general, only few bacteria and no fungi were seen in the tissue sections. The bacteria were mainly Gram-positive cocci and rods, and Gram-negative rods typically located in the degraded muscle fibers or in the interstitium of the muscles. Bacteria were also present in the epidermis and dermis (Fig. 4D,E) but seldom in the adipose tissue.

Bacteriological findings

The pH values of the abdominal material utilized for microbiological analyses ranged from 5.9 to 8.8, with the majority falling within the pH 6 to 7 range across all sampling locations. Cadaverine concentrations ranged from 235 to 1004 mg/kg in the muscle tissue and from 28 to 764 mg/kg in the abdominal tissue (Suppl. data 5).

The aerobic and anaerobic microbial counts for mink abdominal samples spanned from $< \log_{10} 2$ to $\log_{10}$ 7.8 CFU/g and $< \log_{10} 2$ to $\log_{10}$ 7.9 CFU/g, respectively. However, only a few samples, particularly one with a high pH value, exhibited low microbial counts. Concentrations of presumptive clostridial populations ranged

	G1	G2	G3	G4	G5	G6
XT	2		2	2	3	2
XM	1		1	2	2	3
XB	2	2	2	2	2	2
YT	1	2			2	2
YM	1		1	2	1	
YB	1	1		1	2	2
ZT	2		1	3	2	2
ZM	2	1		2	1	2
ZB	2		1	2	2	2

Table 1. Estimated degradation category based on Bradford (BF) soft tissue scores of 3–5 mink in study units matched to the grave number (G1-G6) and location in the grave. (Cadaver box location: X, Y, Z; T: top, M: middle, B: bottom). Green: degradation category 1 with limited changes (BF score between 0 and 50/100). Yellow: degradation category 2 with significant changes (BF score 51–75/100). Red: degradation category 3 with extensive changes (BF score 76–100/100). White cells: missing values. The study unit was not examined due to SARS-CoV-2 RNA RT-qPCR-positive carcasses.

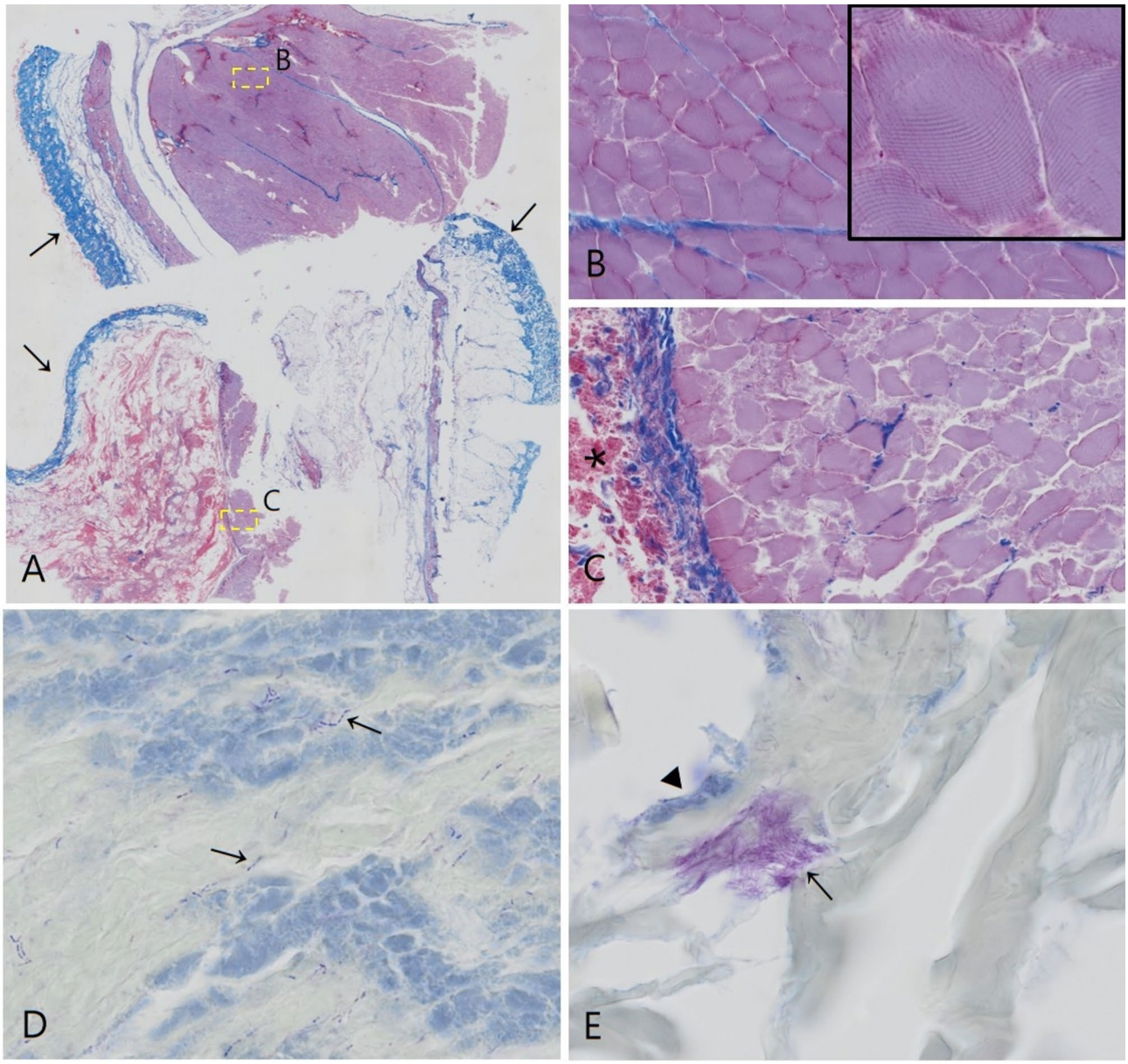

Figure 4. (**A**–**C**) Photomicrographs of pooled samples of three skin blocks with adipose tissue and underlying muscle from mink carcasses from one study unit (G1-XB). Masson trichrome stain; connective tissue (blue), muscle (pink-red), mineralized material (bright red), lipid (unstained). (**D**–**E**) Photomicrographs of tissue sections from a mink cadaver (study unit G5-ZB) with a relatively high number of bacteria in the skin block sample (Brown and Hopp's Gram stain). (**A**) Orientation of epidermis marked by arrow. Yellow boxes indicate area used in panels B and C. (**B**) Well-preserved muscle fibers. Insert: close-up of muscle fiber striation. (**C**) On the right of the image, pieces of well-preserved muscle fibers surrounded by degraded muscle. Mineralized material in subcutis on the left of the image (marked by asterisk). (**D**) Skeleton muscle (blue) with Gram-positive rods (arrows) in the interstitial tissue. (**E**) Aggregate of Gram-negative rods (arrow) in dermis. Epidermis (blue) marked by arrowhead.

from < $\log_{10}$ 2 to $\log_{10}$ 8.1 CFU/g, while concentrations of presumptive clostridial spores varied from < $\log_{10}$ 2 to $\log_{10}$ 6.7 CFU/g.

No significant differences were noted in microbial counts between sampling locations within each site or between the Karup and Holstebro disposal sites. Among the bacterial isolates obtained from the media used for enumerating clostridial vegetative cells and spores, 35 out of 45 and 48 out of 53 isolates, respectively, belonged to the class Clostridia, including species like *Clostridium butyricum*, *Cl. perfringens*, *Paeniclostridium sordellii*, and *Paraclostridium bifermentans*. The remaining 15 isolates remained unidentified. Notably, soil samples exhibited no clostridial spores and presented lower counts of presumptive clostridia compared to the mink samples, with one exception showing $\log_{10}$ 4.3 CFU/g and a neutral pH value of 6.9.

Microbial community analyses revealed that Firmicutes (now Bacillota) comprised the predominant phylum in the mink samples, accounting for 94% of all Operational Taxonomic Units (OTUs) sequenced. This was followed by Proteobacteria (now Pseudomonadota) at 3.6%, Fusobacteria (now Fusobacteriota) at 1%, Bacteroidetes (now Bacteroidota) at 0.8%, and other phyla at 0.7%. Clostridia were the most abundant class, representing 78.9% of all OTUs, followed by Bacilli at 15%. Additionally, Gammaproteobacteria accounted for 3.6%, Fusobacteria for 1%, Bacteroidia for 0.8%, and other classes for 0.7%. At the genus level, the most prevalent genera included *Clostridium* sensu stricto 7, *Hathewaya, Peptostreptococcus*, *Lactobacillus* sensu lato, *Clostridium* sensu stricto 1, and *Peptinophilus*. *Hathewaya* was exclusively identified through culture-independent analysis, although it's conceivable that this genus was also present among the unidentified isolates in the culture-dependent analysis.

Screening for SARS-CoV-2, IAV, AMDV and MCoV

Coronavirus RNA was detected in mink carcass samples, with 12 out of 107 swab samples testing positive for SARS-CoV-2 RNA by RT-qPCR (Table 2). Notably, this diagnostic assay targets a region of only 113 nucleotides within the E-gene. Among the positive swabs, eight were collected from the rectum, while four were collected from the pharynx. Interestingly, only two mink carcasses tested positive in both swab types. Overall, a carcass was considered positive if at least one of the pooled swab types (pharyngeal or rectal) tested positive. These positive samples were found across 7 out of 18 sampling locations from 4 out of 6 graves, with two graves located at the Karup site and two at the Holstebro site.

In a separate analysis, total nucleic acid samples extracted from the mink samples were screened for RNA from influenza A virus (IAV) and mink coronavirus (MCoV), as well as for DNA from Aleutian mink disease virus (AMDV). Results showed that nine out of 42 intestinal pooled swabs tested positive for MCoV, while 8 out of 42 spleen tissue pooled swabs were found positive for AMDV. None of the 39 pooled swabs from lung tissue tested positive for IAV.

Further analysis of partial NS1 sequences (328 nucleotides) revealed that all eight AMDV-positive samples belonged to the 'Saeby' cluster, with 100% identity for the 328 nucleotide sequences in three samples from the same grave at the Karup site. Additionally, one sample from the Holstebro site exhibited sequences identical to an AMD virus collected in 2016 in Northern Jutland.

Regarding the partial MCoV sequence for ORF1a (1690 nucleotides), it showed approximately 91% identity to two Danish MCoV sequences from 2015 and two North American MCoV sequences from 1998. However, the phylogenetic analysis indicated that the MCoV from this study had its own distinct branch in the tree, far from other available MCoV sequences, making it difficult to establish its origin (Fig. 5).

Follow-up RT-PCR analyzes on SARS-CoV-2 positive samples

After conducting conventional reverse transcription (RT-) PCR analyses using 10 different primer combinations on a positive control sample with SARS-CoV-2 RNA, two primer sets yielded positive results. These primer sets targeted the ORF1b and N genes, amplifying fragments of 2000 bp and 1000 bp, respectively. These primer sets were then utilized to evaluate the integrity of the SARS-CoV-2 RNA extracted from the mink samples.

Upon testing nine mink samples and two positive controls with these two assays, only the positive controls produced the 2000 bp amplicon in the ORF1b assay. However, in the N assay, both positive controls and one mink sample were positive. Thus, while it was not possible to amplify fragments of 2000 bp from the mink samples using these primer sets, the 1000 bp amplicon could be produced from a single mink sample. This suggests that the mink-derived RNA was partially degraded but clearly large enough fragments were present to enable the diagnostic assay to yield positive results.

Virus variant determination by WGS and partial sequencing of the spike protein gene from SARS-CoV-2-positive mink samples

Purified RNA from 10 RT-qPCR positive sample pools from grave 2 and grave 3 was examined using WGS and partial sequencing of the spike gene, respectively, to determine the variant of SARS-CoV-2 in the exhumed mink. In 8 out of the 10 sample pools, the mink variant of SARS-CoV-2, with the Y453F substitution in the Spike

Site	SARS-CoV-2 +	SARS-CoV-2 -	Phar. +	Rect. +	Phar. + & Rect. +	Phar. + or Rect. +	Positive sampling spots	N
Grave 1	0	18	0	0	0	0	0	18
Grave 2	6	12	3	3	1	4	3	18
Grave 3	4	14	1	3	1	2	2	18
Grave 4	1	17	0	1	0	1	1	18
Grave 5	0	18	0	0	0	0	0	18
Grave 6	1	16	0	1	0	1	1	17
Holstebro	10	44	4	6	2	6	5	54
Karup	2	51	0	2	0	2	2	53
Total	12	95	4	8	2	8	7	107

Table 2. Locations of the SARS-CoV-2 RT-qPCR tests. +: positive test result, -: Negative test results, *Phar.* Pharyngeal pool of swabs, *Rect.* Rectal pool of swabs, and *N* number of swabs tested.

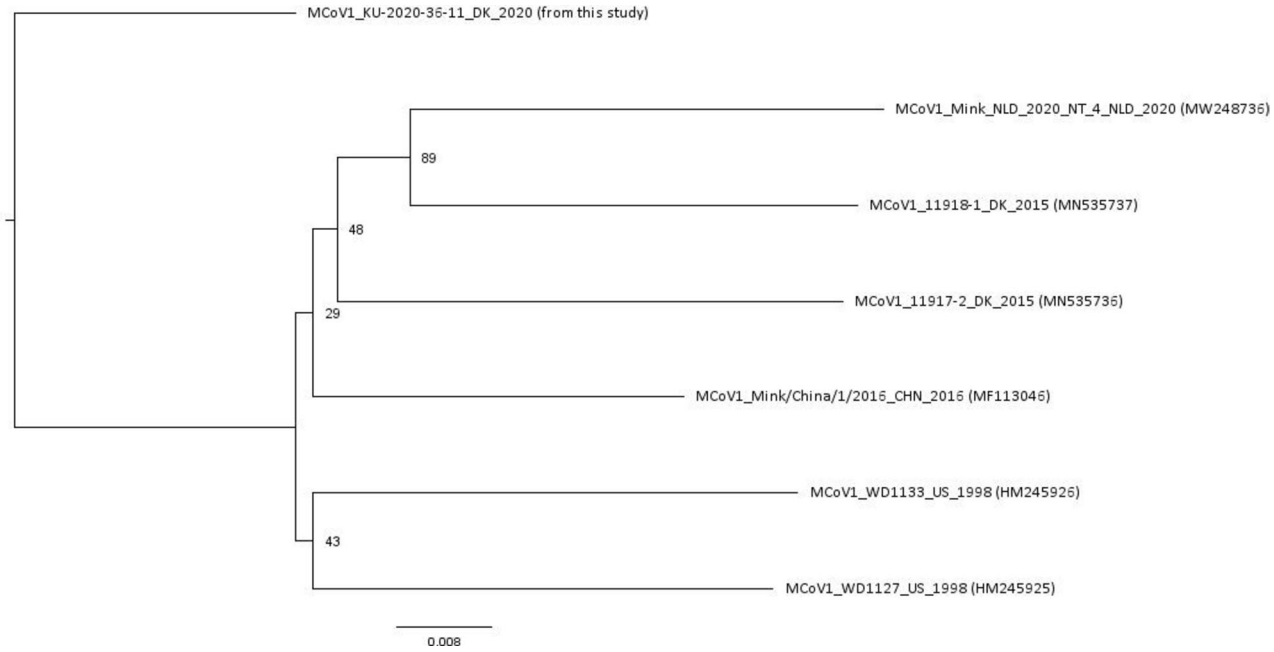

Figure 5. Phylogenetic tree with MCoV sequences. The tree is based on 1673 nt from the MCoV ORF1a sequence. The case virus sequence (KU-2020-36-11_DK_2020) does not cluster with the other MCoV sequences available in Genbank and therefore the origin of this virus cannot be established from the few MCoV sequences available. The tree algorithm was Neighbor Joining and the distance measure Jukes-Cantor with 1,000 bootstrap replicates. The tree was visualized by FigTree v1.4.5.

protein, was found, which belongs to pangolin Lineage B.1.1.298[15]. In the remaining sample pools, it was not possible to determine the variant of SARS-CoV-2. Complete viral genome sequencing was not achieved for any of the samples, with missing regions ranging from 3600 to 7700 nt (out of about 30,000 nt).

Infectivity of SARS-CoV-2 from mink carcasses

Samples from eight mink carcasses, comprising three throat swabs, three rectal swabs, and two lung material samples, underwent extensive virological examination using a cell culture assay setup. These samples were inoculated onto Vero E6 cells and cultured for 5 passages. Cytopathogenic effect (CPE) was assessed by microscopy, and the samples were tested in the E-Sarbeco RT-qPCR assay and the confirmatory N-gene RT-qPCR assay after each passage.

One sample, a rectal swab from grave 3, yielded a high Ct value (36.21) in the confirmatory RT-qPCR after the first passage, indicating a low level of viral RNA in the original material. However, this sample tested negative for CPE in the final reading at the 5th passage. All other samples tested negative in both the diagnostic E-RT-qPCR and the confirmatory N-gene RT-qPCR. The samples exhibited varying degrees of CPE, with some showing apparent toxicity under microscopic examination, albeit decreasing with each passage.

Discussion

The major findings of this study are twofold: first, only limited degradation of mink carcasses occurred after approximately six months of burial; second, SARS-CoV-2 RNA was detected in mink carcass samples, but without detectable infectivity.

Regarding the burial scenario, the large-scale disposal of mink carcasses led to the eruption of carcasses from the graves due to inadequate burial procedures. At the Holstebro site, the lack of barriers to prevent longitudinal movement resulted in high pressures on the mink layer at one end of the grave, causing longitudinal carcass mass movement. Conversely, at the Karup site, vertical soil barriers were constructed, resulting in carcass movements to the sides of the grave segments. This issue might have been mitigated by placing barriers above the carcass mass in the graves.

Heterogeneity among the graves was reflected in the variability of pH values, suggesting differences in the amounts of slaked lime among samples. These findings indicated varied local physicochemical conditions within the graves, likely contributing to the observed differences in mink carcass degradation. Carcass samples collected just below, above, or in the middle of the slaked lime layers showed minimal pH increases. During excavation, puddles of water observed above the top slaked lime layer and water intrusion into gas sampling probes installed in the deeper parts of the cover soil indicated that the slaked lime layer partially or completely prevented atmospheric air and rainfall intrusion into the mink burial layer. The accumulation of water may have been due to the compressed slaked lime reducing permeability or creating a capillary barrier effect between the sandy cover soil and the slaked lime, potentially decreasing the decomposition rate of the mink carcasses. It is

unknown whether the protective effect of the slaked lime would have persisted long-term if the mink had not been exhumed after six months.

The limited anaerobic decomposition was supported by gas investigations showing aerobic conditions in the cover soil and limited formation and emission of CH_4, N_2O, NH_3 and H_2S from the mink graves. However, some soil profiles exhibited elevated CO_2 concentrations and reduced O_2 levels compared to background measurements, indicating some degree of aerobic respiration, likely by bacteria, within the disposed mink carcasses. Overall, the gas observations corroborated the visual findings of limited carcass decay. This is consistent with findings by Schotsmans et al.[16], who studied the decay of porcine carcasses covered with lime and buried for six months, as well as reports of well-preserved human remains exhumed from mass graves without slaked lime even after 21 years[17].

Differences between mink farms in the time periods from culling to burial likely influenced the level of decay observed after six months. This variability may explain why carcass degradation, presented as Bradford scores or degradation categories, did not correlate with the location of the carcasses in the graves.

Decay of mink carcasses

The carcass decay process occurs in three stages. In the first stage, the abrupt drop in oxygen tension initiates tissue autolysis, causing the release of cellular enzymes. During the second stage, decay proceeds due to the growth of anaerobic bacteria and the release of bacterial enzymes, which are responsible for most tissue destruction. The third stage of decomposition may be initiated if the carcass is exposed to insects, which was not the case in our study[18]. The degree of tissue destruction is influenced by the bacterial burden, with levels of 10^5 bacteria/g considered critical for the risk of infection and/or failure of wound closure in burn wound biopsies[19].

In the human colon, the decreased oxygen tension during the first 2–3 days postmortem causes a shift from aerobic to anaerobic bacterial proliferation, with anaerobic bacteria spreading from the intestine to other parts of the body via the blood vessels. Temperature greatly impacts bacterial proliferation, which is reduced at temperatures below 4 °C in unburied animals. This reduction in bacterial growth is expected to be even more pronounced in buried carcasses[18,20].

Since the mink carcasses were buried in November 2020, the cool environment during the winter and spring likely inhibited bacterial growth, partially explaining the low number of bacteria observed in the histological skin block sections. As the slaked lime did not significantly affect the pH levels in most mink carcasses, it is unlikely that lime application had a major impact on bacterial numbers in the carcasses.

The head region of the mink exhibited the most advanced decay, likely due to bacterial activity originating from the oral cavity. These bacteria can migrate into the esophagus and respiratory tract, leading to accelerated decomposition rates of thoracic organs compared to those in the abdomen. The stomach was seldom recognizable, likely a result of autodigestion by gastric acid and bacterial degradation. In contrast, the intestines were often identifiable, with limited degradation of the intestinal connective tissue, potentially due to reduced growth of intestinal bacteria.

The subcutaneous adipose tissue was often not macroscopically visible, which was unexpected since farmed mink typically have good body condition in the autumn when they were culled. However, when the skin blocks were submerged in formalin, the adipose tissue "reappeared," suggesting that the observed reduction in adipose tissue thickness could be due to desiccation, followed by rehydration during formalin fixation.

In humans, adipocere (corpse wax) can develop due to the hydrolysis and hydrogenation of body fat, particularly when corpses with substantial subcutaneous and abdominal fat are buried in damp conditions. Early in adipocere formation, fatty tissue turns into a creamy, greasy substance, which later hardens due to the crystallization of fatty acids[4,5]. Although we did not observe the formation of subcutaneous adipocere in the mink, several carcasses displayed abdominal adipose tissue that had transformed into "fat pearls/grains," which might eventually develop into adipocere.

Microbiological findings and SARS-CoV-2

Cadaverine, a compound originating from the microbial decarboxylation of the amino acid lysine[7,21], is commonly associated with the decay process. The observed cadaverine concentrations in the analyzed materials indicate that proteolytic activity had occurred. Our microbiological analyses show that primarily vegetative cells or spores of anaerobes belonging to the phylum Firmicutes, particularly *Clostridium* sensu lato, were present in the abdomens of the cadavers. This finding was supported by the microbiome analysis, although the proportion of taxa varied between culture-dependent and independent analyses.

In contrast to the gut microflora in living mink, the abdominal content of the exhumed mink showed a higher relative abundance of Firmicutes (e.g., *Lactobacillus* sensu lato and *Enterococcus* spp.) and a lower relative abundance of the class Gammaproteobacteria (e.g., *Escherichia* spp. and *Proteus* spp.)[8]. This shift in microbial populations is indicative of the decomposition process under the anaerobic conditions present in the graves. Moreover, the soil samples generally contained low levels of bacteria, likely due to the sandy characteristics of the soil, which typically have low concentrations of nutrients and sub-optimal conditions for bacterial growth compared to richer clay soils. This might have contributed to the limited microbial activity and subsequently slower decomposition rates observed in the mink carcasses.

The distribution of mink carcasses that tested RT-qPCR-positive for SARS-CoV-2 viral RNA across several sampling locations suggests that these carcasses originated from mink farms infected with SARS-CoV-2 at the time of culling. Due to the lack of registration at the time of burial, it was not possible to trace the sampled carcasses back to their respective farms. The low temperatures and limited degradation of the mink carcasses likely inhibited the degradation of intact virus particles, thus partially preserving the viral RNA within them. Low temperatures and moisture levels have been shown to enhance the survival of SARS-CoV-2[22–24]. Soil temperatures

in Denmark, measured at one-meter depth representative for the two weather stations closest to the burial sites November 2020–May 2021, ranged from 2.9 to 8.9 °C[25].

Overall, the Ct levels measured in the samples (Ct 28–40) indicate low levels of viral RNA. A subsequent bioassay for virus infectivity did not yield positive results, indicating the absence of infectious SARS-CoV-2 particles. This supports findings by others that SARS-CoV-2 RNA can persist longer than infectious particles[22], as even a single break in the RNA genome can render the virus non-infectious. Furthermore, testing for RNA preservation showed that cDNA fragments of 1000 bp could be amplified, but not those of 2000 bp, indicating that while viral RNA was present, it was partially degraded.

Both Aleutian mink disease virus (AMDV) and mink coronavirus (MCoV) genomic material were detected by (RT)-qPCR from the exhumed mink carcasses. AMDV belongs to the Parvoviridae family[26] and is known for its extreme resistance to environmental stress, including high temperatures and exposure to various chemicals[27,28]. This remarkable stability makes AMDV difficult to eliminate from contaminated materials and facilitates its spread within and between mink farms[29,30]. The detection of AMDV genomic material in the mink carcasses likely reflects the resilience of this virus. However, it remains uncertain whether the analyzed samples contained infectious AMDV particles. To determine the presence of infectious particles, an in vivo experiment (bioassay) would be necessary. Such an assay would help establish whether the genomic material detected is, at least in part, within viable viruses that are capable of causing infection.

Mink coronavirus (MCoV) belongs to the subgenus *Minacovirus* within the genus *Alphacoronavirus*. Like SARS-CoV-2, MCoV is an enveloped RNA virus, which typically reduces its environmental stability and survival. This study was unable to determine if the MCoV detected in the mink carcasses was infectious. A case–control study conducted on Danish mink farms in 2015 revealed a high prevalence of MCoV in animals with and without diarrhea[31]. Currently, only six full genome sequences of MCoV are available in GenBank, all showing relatively low similarity to each other (89.20–92.54%). The MCoV identified in this study also exhibited significant genetic divergence from the other available sequences. Specifically, in the sequenced region of the genome (1673 nt out of the 12,057 nt comprising ORF1a), the MCoV was substantially different from the other known sequences, making it impossible to establish the origin of the detected virus.

In conclusion, this study highlights the necessity of clearly defining the objectives for mass burial of dead animals. The use of slaked lime around carcasses can mitigate the risk of environmental contamination by leachate from dead animals, potentially reducing the risk of SARS-CoV-2 contaminating groundwater[24]. This benefit assumes that the burial process avoids heterogeneities that could lead to pressure build-up and surface eruptions. However, the addition of slaked lime may also slow the rate of cadaver decomposition, potentially prolonging the viability of pathogens that caused the outbreak.

Importantly, the study demonstrated the detection of SARS-CoV-2 RNA in mink carcasses after six months, although no infectious virus particles were identified. This finding suggests that while viral RNA can persist, infectivity may not. Future mass burial scenarios must balance environmental contamination concerns with the potential for prolonged survival of infectious agents. The choice of burial site and soil characteristics will be crucial in this decision-making process, as illustrated by a recent study on SARS-CoV-2-related human mass burials and their risk of groundwater contamination[32]. Overall, this study underscores the complexity of managing mass burials to control environmental risks and pathogen viability, emphasizing the need for careful planning and consideration of site-specific conditions.

Materials and methods

Burial site description

Two military sites with sandy soils[33,34] were used for the burial of culled mink: one in Kølvrå near Karup and one in Nr. Felding near Holstebro in the western part of Denmark (Fig. 1A). Burial guidelines specified that graves should be approximately 3 m wide and 2.5 m deep, with a capacity of around 60,000 mink per 100 m, equivalent to approximately 300–350 tons of mink per 100 m (Suppl. data 11). The length of the graves varied at the Karup site from 7.5 to 300 m and at the Holstebro site from 24 to 164 m. At the base, a 5 cm layer of hydrated lime was applied, followed by a 0.5-m-thick layer of mink carcasses. The top layer consisted of hydrated lime amounting to 10–20% of the total mink mass. The graves were 3 m deep at the Karup site and 2.5 m deep at the Holstebro site. The carcasses were covered with approximately 2 m of soil. Both gravesites where surrounded by game fence with fox protection to inhibit digging activity of scavengers.

On-site observations of burial sites

Before and during the exhumation of the carcasses, the graves underwent visual inspections. Physical and other characteristics of the burial sites were documented, including illustrative photos. Three representative graves at each of the two disposal sites were selected for sampling, taking into consideration the observations made and the geographical location of the graves.

Gas investigations

Gas formation, transport, and surface emission (CH_4, CO_2, H_2S, N_2O and NH_3) were investigated through surface screenings, measurements of gas composition in the cover soil of the mink graves, and assessment of surface gas fluxes and emissions across the entire site.

Visual inspections and CH_4 surface concentration screenings were conducted to detect cover irregularities (e.g., settlement damage, surface cracks, vegetation development) and identify potential high-emission areas. A Laser One Portable Methane Leak Detector (Huberg, Italy) was employed for the screening (1–10,000 ppm CH_4, with a response time of 3.5 s), and surface CH_4 concentrations were continuously recorded a few centimeters above the ground along the edges and at the center of each mink grave. Locations with elevated CH_4

concentrations were marked for further investigation, and cracks and fissures in the soil cover were surveyed using the laser detector.

Vertical gas concentration profiles in the soil cover of the mink graves were generated by installing gas probes (15 mm ID) at different depths below the surface (20, 40, 60, 80, 100, 120, 140–160 cm) (Suppl. data 3.6). Gas composition was analyzed using a portable gas analyzer Biogas 5000 (CH_4, CO_2, O_2, N_2 (%vol.) and H_2S (ppm)) (Geotechnical Instruments, Warwickshire, UK) or a photoacoustic gas monitor INNOVA 1512i (LumaSense technologies A/S, Denmark) (CH_4, CO_2 and N_2O (ppm))[35,36].

Surface gas emissions (CH_4, CO_2, N_2O and NH_3) from the mink graves were determined using static flux chambers (30 cm ID, 21 cm height) placed next to the gas probes[35,36]. Gas concentrations (1 sample per min for minimum 5 min) were analyzed using INNOVA 1512i (ppm) and cavity ring-down spectroscopy (CRDS) analyzers (ppb) (G2203 and S/N JADS2001, Picarro, Inc., Santa Clara, CA)[37,38]. The total CH_4 emissions from mink disposal sites were quantified using a mobile tracer dispersion method as previously described[37,39].

Measurements of pH in soil mixed with slaked lime

Samples of soil containing slaked lime were collected for pH measurements. About two liters of soil placed above and below the layer of mink carcasses were collected, respectively and placed in plastic bags. The soil sample was mixed by manipulating the bag by hand for 10 min. Eight grams of soil sample were transferred to a sterile 50 ml Techno Plastic Products AG (TPP©) centrifuge tube (Merck, Darmstadt Germany), and 40 ml of sterile water was added to limit the headspace in the tube. After 30 s of vigorous shaking, the soil sample was left at room temperature for one hour with a cap on. Afterwards, the sample tube was shaken again and left for sedimentation and the liquid phase was removed for pH measurement using a calibrated pH-meter (913 pH Meter, Methrom).

Sampling and examination of mink carcasses

At the disposal sites, three to five mink carcasses were collected and transferred to hard transparent plastic boxes with lids. Used boxes were cleaned and disinfected with Virkon™ S solution (LANXESS Corporation) between sampling events. At each of the six selected graves (three at the Holstebro site and three at the Karup site), three sampling locations were marked, and three samples were taken from each location—namely, the top, middle, and bottom levels of the grave. Thus, a total of 54 boxes with mink carcasses (study units) were obtained. Details about the sampling are provided in Suppl. data 10. A wheel loader excavator carefully removed topsoil deposited on the grave until the first traces of slaked lime were seen. Samples of soil mixed with slaked lime and mink carcasses were then collected. At each of the three levels of the grave, the aim was to randomly sample three to five individual mink carcasses, which were placed in the transport boxes together with plastic bags containing mixed soil from the top and bottom layers.

Pharyngeal and rectal swabs were obtained from each carcass in a sampling unit and pooled for each swab type. Swabs were placed in sterile plastic tubes for RT-qPCR testing for SARS-CoV-2 (see methodology below). For biosafety reasons, only carcasses that tested negative for SARS-CoV-2 in the RT-qPCR were examined further. Boxes were cleaned on the outside with high-pressure water and then disinfected with Virkon™ S solution before being placed inside a sealed plastic bag. All samples were transported immediately to the Statens Serum Institut (swab samples) and the University of Copenhagen (soil samples and plastic boxes with mink carcasses). Sample transport time varied from six to ten hours until the boxes and swabs were placed in cold storage (2–8 °C).

The closed boxes were X-rayed on the day after arrival at the University of Copenhagen to give an estimate of the number of skeletons/carcasses in each box. After receiving the SARS-CoV-2 RT-qPCR test results, the macroscopical examinations were initiated on RT-qPCR-negative mink carcasses two to four days after sampling. Boxes with SARS-CoV-2 PCR-positive mink carcasses were not examined macroscopically. The mink carcasses in the boxes from each grave were examined in an arbitrary order by the same veterinary pathologist.

A total of 44 study units (i.e. boxes) with three (n = 37) or five (n = 7) mink carcasses were examined macroscopically. The presence of fluid or insects in the boxes was recorded. It was noted whether the carcass was intact, i.e. no visible rupture of skin barrier or absence of body parts.

For each mink, the degree of degradation of the soft tissues was scored using the Bradford (BF) scoring system developed by Schotsmans et al.[16], who used it for evaluating degradation of individual swine carcasses. The BF score is a 0 to 100 scale, where 0 represents minimal decomposition changes and 100 correlates with maximal changes. The BF scoring system was modified to fit the present study. During necropsy, the condition of the soft tissues was scored from 0–3:

- 0 = represented minimal changes in the form of mild discoloration and mild signs of decay of the carcass
- 1 = some changes, with evident decay of the carcass, where the examined area is only partially intact, i.e. the tissue could still be identified, but had lost its usual structure
- 2 = widespread changes where the carcass was no longer intact due to advanced decay, adipocere can be seen at this stage
- 3 = extensive changes with advanced decay, where the soft tissues had dissolved.

For the BF scoring, the carcass was divided into head, torso and extremities and the following soft tissues were scored separately: integument (skin and fur), subcutaneous adipose tissue (not scored on the head), skeletal muscles and ligaments.

The decomposition grade of the internal organs (heart, lung, diaphragm, liver, stomach, intestine, spleen, kidneys, abdominal fat) was scored using the same definitions as in the BF soft tissue scoring system. A total soft tissue degradation BF score was estimated per study unit, i.e. the sum of the BF scores of all mink in the box. These total scores were then divided into three degradation categories according to Schotsmans et al.[16],

where 1 represented limited changes of the soft tissues of the head, torso and extremities (BF score between 0 and 50/100), 2 represented significant changes (BF score 51–75/100); and 3 represented extensive changes (BF score 76–100/100).

Histological analyses

Histological analyses were conducted on a block of skin with subcutaneous adipose tissue and underlying muscle from the thigh of each mink carcass. Tissue samples from all carcasses in each study unit were pooled and fixed in 10% neutral buffered formalin, processed using routine histological methods, embedded in paraffin wax, and cut into 3–5 µm thick sections. The sections were mounted on conventional or superfrost plus glass slides and stained with four different histochemical stains following protocols outlined in Schotsmans et al.[16] and Salihbegović et al.[17]. Hematoxylin and eosin stains were used to demonstrate cell preservation and overall tissue structures. Masson's trichrome stain was employed to highlight tissue structures, particularly muscle and collagen. Brown and Hopp's Gram stain and periodic acid-Schiff stain were utilized to visualize bacterial cells (Gram-negative/Gram-positive) and fungi, respectively. Given the similarity of histological findings within and between pooled samples from different study units, an arbitrary selection of slides was examined.

Microbiological analyses

The following samples were collected from the mink carcasses (samples were pooled from all mink in a study unit):

For virological analyses, tissue samples from the intestine, spleen or liver, and lung were collected for (RT)-qPCR examination for Mink Coronavirus (MCoV), Aleutian Mink Disease Virus (AMDV), and Influenza A Virus (IAV). Additional pharyngeal and rectal swabs, as well as lung tissue, were sampled from each mink in the boxes with SARS-CoV-2 RT-qPCR-positive mink for further SARS-CoV-2 analysis, such as determination of infectious virus (see details below). Intestines, liver, and muscle (quadriceps femoris) were also sampled for bacteriological analysis, with muscle samples additionally tested for cadaverine measurements.

SARS-CoV-2 RT-qPCR testing

Paired pools of either pharyngeal or rectal swabs were tested for SARS-CoV-2 viral RNA. Each sample pool consisted of three individual swabs from three mink carcasses. The samples were released from the swabs using phosphate buffered saline and viral RNA was extracted from them using a MagNaPure 96 robot with MagNA Pure 96 DNA and Viral NA Small Volume Kit (Roche, Basel, Switzerland) and assayed using the SARS-CoV-2 E-gene RT-qPCR assay[40].

Follow-up RT-PCR analyses on SARS-CoV-2 positive samples

From the ARTIC primer set for SARS-CoV-2 (v3, https://github.com/artic-network/artic-ncov2019/tree/master/primer_schemes/nCoV-2019/V3), ten primer pairs were initially selected. These ten primers pairs targeted the ORF1a, ORF1b, S gene, or N gene and amplified fragments of approximately 1000, 2000, or 4000 base pairs (bp) (Suppl. data 8). Upon testing the primers on a known positive control, two out of the ten primer pairs, targeting ORF1b and N, respectively, yielded positive results. Subsequently, these two primer pairs were used to test nine mink samples (Suppl. data 8).

cDNA was synthesized from the extracted RNA using the SuperScript III First-Strand Synthesis System for RT-PCR (Invitrogen, San Diego, CA, USA) and amplified by PCR using the AccuPrime™ Taq DNA Polymerase, high fidelity kit (Invitrogen, San Diego, CA, USA). This two-step RT-PCR was performed according to the manufacturer's protocols with the modification that the cDNA synthesis step used an incubation at 50 °C for 90 min before terminating the reaction at 85 °C for 5 min. The PCR products were separated by agarose gel electrophoresis, and each sample was considered positive, if a band of the expected size was observed. No products were obtained in negative controls (water) assayed in parallel.

Sequencing of SARS-CoV-2 and Spike protein-gene

For whole genome sequencing, RNA from RT-qPCR pools was sequenced using the nCoV-2019 sequencing protocol V.1[41]: https://www.protocols.io/view/ncov-2019-sequencing-protocol-bp2l6n26rgqe/v1) modified for Artic primer scheme v3 (https://github.com/artic-network/artic-ncov2019/tree/master/primer_schemes/nCoV-2019/V3) and Illumina MiSeq sequencing. Libraries were generated using the Nextera XT DNA Library Prep kit as recommended by the manufacturer and sequenced on a MiSeq instrument (Illumina, San Diego, CA, USA) using MiSeq® Reagent Kit v2 (500 cycle) generating 250-bp paired-end reads. Reads were mapped to a wt-SARS-CoV-2 reference (NC_045512.2) using CLC Genomics Workbench v.21.0.4 (Qiagen, Aarhus, Denmark).

A method for partial spike gene sequencing amplification of a 1049 nucleotides (nt) fragment, including part of the receptor binding domain (nt 22,799–23,847, aa413-761 [NC_045512.2_Wuhan-Hu-1], Suppl. data 9), was modified for library preparation and Nanopore sequencing using a three-step PCR amplification procedure. The initial one-step RT-PCR was originally developed for Sanger sequencing (https://www.protocols.io/view/sanger-sequencing-of-a-part-of-the-sars-cov-2-spik-j8nlk4dx6g5r/v1)[42]. Barcoding PCR and library preparation were performed following the Oxford Nanopore Protocol for PCR barcoding (96) amplicons (SQK-LSK110, Oxford Nanopore Technologies) with the PCR Barcoding Expansion 1–96 (EXP-PBC096, Oxford Nanopore Technologies). Sequencing was performed on a GridION Mk1 using a MinION Flow Cell (R9.4.1, FLO-MIN106D, Oxford Nanopore Technologies). Only reads between 900 and 1200 nt were used for further analysis (for a detailed description see[43]). Reads were mapped to a reference set consisting of the 1049 nt Spike-gene fragment derived from wt-SARS-CoV-2 (NC_045512.2) and B.1.1.298 (hCoV-19_Denmark_DCGC-3024_2020_EPI_ISL_616802)

using CLC Genomics Workbench v.21.0.4 (Qiagen, Aarhus, Denmark). For both WGS and Spike sequencing consensus sequences were analyzed for mutations using Nextclade[44].

Cell culture infectivity assay

Individual follow-up samples from each mink carcass in the original positive pools were examined for viral content using diagnostic RT-qPCR to identify positive samples at the individual animal level. From this, the most suitable sample material was selected for extended virological examination in cell assays. The selected samples were processed in cell culture medium supplemented with antibiotics and then divided into sterile filtered and unfiltered fractions. Each sample was tested on a cell culture plate (Vero E6 cells) in four different sets, with unfiltered and filtered fractions in undiluted and 1:10 diluted setups (i.e., final dilution of each sample was 1:10 and 1:100 with and without sterile filtration). All samples were inoculated by adsorption inoculation, involving close contact between the sample and cell layer for 1 h at 37°C incubation. The samples were then aspirated to avoid a toxic effect, cell culture medium added, and the cell culture plate incubated at 37°C for 72 h. After incubation, the plate was frozen for passage and inoculation onto fresh cells. Passaging was repeated for a total of 5 passages. From each passage, material was sampled for testing in the SARS-CoV-2 E-gene RT-qPCR assay.

Bacteriological analyses

As the individual mink carcasses were mostly intact, bacteriological analysis was performed on core tissue parts. A total of 44 samples of pooled material from the abdomen (ventriculus, ilium, colon, and liver when present) were used for various culture-dependent analyses, with eighteen of these utilized for microbiome analyses. The sampled tissue material was homogenized using sterile scissors, and 10 g of homogenized sample were transferred aseptically into a Stomacher bag with a filter (Bagsystem, Interscience). Buffered peptone saline was added in a 1:10 ratio before homogenization in a Stomacher (Stomacher 400, Seward) operated at maximum speed for 2 min. Approximately 1–2 g of each sample was collected before and after adding the diluent and stored at − 80 °C for later DNA extraction and cadaverine measurement. Serial dilutions were made for every sample, with an additional serial dilution performed after the samples were heat-treated (80 °C for 10 min) to determine the number of clostridial spores. pH was measured in homogenized material as described above.

Enumeration of bacterial concentrations were performed on agar plates using standardized and validated methods[45,46]. Total aerobic and anaerobic bacterial counts were enumerated on Plate Count agar (PCA, Oxoid) incubated at 30 °C for 72 h. Iron sulfite agar (Oxoid) was used for enumeration of sulfite reducing clostridia and their spores by incubation anaerobically in airtight containers (Oxoid™ AnaeroGen™, Thermo Scientific™) at 37 °C for 48 h and including a positive control (*Clostridium perfringens*) and a negative control incubated aerobically. Similar bacterial enumerations were also performed on six soil samples.

Fifteen representative isolates from carcass tissue originating from one grave were obtained by picking colonies randomly from iron sulfite agar plates and sub-cultured onto blood agar plates (10% Ox blood, Håtunalab) to check for purity and subsequent identification by MALDI-TOF MS (BioMérieux, France). Additionally, 20 colonies were selected from aerobically incubated PCA plates, i.e. 10 arbitrarily selected isolates and 10 isolates representing different colony morphologies, and identified by MALDI-TOF MS (BioMérieux, France).

Measurement of cadaverine

Cadaverine was measured in 18 samples of pooled abdominal content (ranging from 0.1 to 1.1 g) and 15 samples of pooled quadriceps muscles (ranging from 1.5 to 5.1 g). All samples were stored at − 80 °C until measurements were performed by the Danish Technological Institute. Perchloric acid was used for extraction followed by three steps: solid-phase ion exchange purification using Oasis WCX 60mg 3CC columns (Waters, Denmark), chromatographic separation using reverse-phase columns with heptafluorobutyric acid as an ion-pairing agent, and detection using tandem mass spectrometry by electrospray ionization[47] and references quoted therein).

Microbial community analysis

This analysis was conducted on three samples from each grave in duplicate (N = 36). Three sterile water samples were used as negative controls, and a custom mock community was used for extraction. The DNA extractions were done using a Bead-Beat Micro AX Gravity kit (A&A Biotechnology, Poland) following the manufacturer's instructions with minor modifications. Two additional bead-beating steps at maximum power for 45 s were added and an additional centrifugation step of the supernatant after bead beating for 5 min at 12,000 rpm was added, before transferring the supernatant to Micro AXD columns (Bead-Beat Micro AX Gravity kit). The quality of the DNA was assessed using a NanoDrop One Spectrophotometer (Thermo Scientific), and the DNA concentration was measured with a Qubit dsDNA HS kit on a Qubit 2.0 (Thermo Scientific).

The microbial community analysis on the extracted DNA was performed by DNAsense (Aalborg, Denmark). Gene amplicon sequencing targeting the 16S rRNA gene v4 region was performed on a MiSeq (Illumina, USA). Briefly, up to 10 ng of extracted DNA was used as template for PCR amplification with primers targeting the bacteria/archaea 16S rRNA gene variable region 4 (abV4-C: [515FB] GTGYCAGCMGCCGCGGTAA and [806RB] GGACTACNVGGGTWTCTAAT[48]. Each PCR reaction (25 µL) contained (12.5 µL) PCRBIO Ultra mix and 400 nM of each forward and reverse tailed primer mix. PCR was done by initial denaturation at 95 °C for 2 min, 30 cycles of amplification (95 °C for 15 s, 55 °C for 15 s, 72 °C for 50 s) and a final elongation at 72 °C for 5 min. The resulting amplicon libraries were purified using the standard protocol for CleanNGS SPRI beads (CleanNA, NL) with a bead to sample ratio of 4:5. DNA was eluted in 25 µL of nuclease free water (Qiagen, Germany) and concentration was measured using Qubit dsDNA HS Assay kit (Thermo Fisher Scientific, USA). Gel electrophoresis using Tapestation 2200 and D1000/High sensitivity D1000 screentapes (Agilent, USA) was used for validation of product size and purity of a subset of sequencing libraries, prepared from the purified amplicon libraries using

Site	Lung tissue pools	IAV positive	Spleen tissue pools	AMDV positive	Intestinal pools	MCoV positive
Grave 1	9	0	9	3	9	4
Grave 2	3	0	3	0	3	0
Grave 3	5	0	6	0	6	2
Grave 4	8	0	8	0	8	1
Grave 5	9	0	9	3	9	1
Grave 6	5	0	7	2	7	1
Holstebro	17	0	18	3	18	6
Karup	22	0	24	5	24	3
Total	39	0	42	8	42	9

Table 3. Number of positive samples and types of material from each grave. *IAV* Influenza A virus, *AMDV* Aleutian mink disease virus, *MCoV* Mink coronavirus.

a second PCR. Each PCR reaction (25 µL) contained PCRBIO HiFi buffer (1×), PCRBIO HiFi Polymerase (1 U/reaction) (PCRBiosystems, UK), adaptor mix (400 nM of each forward and reverse) and up to 10 ng of amplicon library template. PCR was done by initial denaturation at 95 Quast 2013 for 2 min, 8 cycles of amplification (95 °C for 20 s, 55 °C for 30 s, 72 °C for 60 s) and a final elongation at 72 °C for 5 min. The resulting sequencing libraries were purified as described above. The purified libraries were pooled in equimolar concentrations and diluted to 2 nM. The samples were paired-end sequenced (2 × 300 bp) on a MiSeq (Illumina, USA) using a MiSeq Reagent kit v3 (Illumina, USA) following the standard guidelines for preparing and loading samples on the MiSeq. > 10% PhiX control library was spiked in to overcome low complexity issues often observed with amplicon samples. Taxonomic classification was achieved using the SILVA 132 database[49]. Forward and reverse reads were trimmed for quality using Trimmomatic v. 0.32[50] with the settings SLIDINGWINDOW:5:3 and MINLEN: 225 . The trimmed forward and reverse reads were merged using FLASH v. 1.2.7[51] with the settings -m 10 -M 250. The trimmed reads were dereplicated and formatted for use in the UPARSE workflow[52]. The dereplicated reads were clustered, using the usearch v. 7.0.1090 -cluster_otus command with default settings. OTU abundances were estimated using the usearch v. 7.0.1090 -usearch_global command with -id 0.97 -maxaccepts 0 -maxrejects 0. Taxonomy was assigned using the uclust classifier as implemented in the assign_taxonomy.py script in QIIME[53] and the SILVA database, release 132[54]. All bioinformatic processing was done via RStudio IDE (1.4.1717) running R version 4.1.0 (2021–05-18) and using the R packages: ampvis (2.7.8)[55], tidyverse (1.3.1), seqinr (4.2.8), ShortRead (1.50.0) and iNEXT (2.0.20)[56,57].

Detection and sequencing of viruses pathogenic to mink

A total of 39 lung tissue pools, 42 spleen tissue pools, and 42 intestinal pools (part of intestine with content) were sampled from mink carcasses exhumed from the six graves (Table 3).

Total RNA was extracted from lung tissue pools and intestinal pools using the RNeasy mini kit (QIAGEN, Hilden, Germany) following the manufacturer's instructions. Total DNA was extracted from spleen tissue pools using the QIAamp DNA mini kit (QIAGEN) according to the manufacturer's instructions. The extracted RNA and DNA were stored at − 80 °C and − 20 °C, respectively until use. RNA extracted from lung tissue pools was screened for IAV using a RT-qPCR assay targeting the matrix gene[58,59]. DNA extracted from spleen tissue pools were screened for AMDV using a qPCR targeting the left ORF of the AMDV genome[60]. RNA samples extracted from intestinal pools were screened for MCoV by an RT-qPCR assay targeting the 3'-end of ORF1a (MCoV-Fw: 5'-CATGGAAGAAAACGCCTGGC-3´, MCoV-Rev: 5'-TGCGAACTACCGTCCTTCAC-3´, probe: 5'-FAM-AGATGTTGAAACCATGTTTGGAAAACGCAGTG – 3'BHQ-1). Positive and negative controls were included in all nucleic acid extractions and qPCRs.

All qPCR positive AMDV samples were selected for sequencing a part of the NS1 gene (328nt). The primer sequences and conventional PCR conditions have previously been described[61,62]. The conventional PCR primers were used as sequencing primers. One positive MCoV sample was selected for sequencing. The cDNA synthesis and conventional PCR conditions were performed as previously described[63] with a minor modification to the cDNA synthesis step that was extended to three hours. The primer pair targeting ORF1a of MCoV yields a PCR product of 1,749 bp (F8989: 5'- GTACACACCACCAACTGTCAGTG- 3' and R10576: 5'- GTAGGTGCGGTC AAGTTGTTAGC- 3'). The conventional PCR primer pair and one internal primer (F9725: 5'-GCTCGCTCT AATGGTTACACTGAAT- 3') were used as sequencing primers. The purified PCR products were sequenced at LGC genomics GmbH (Berlin, Germany). The raw sequencing data was assembled and analyzed using the commercial software CLC Main Workbench v. 20.0.4.

Data availability

Data are provided within the manuscript or supplementary information files. Additional sequence data may be provided by the corresponding author.

Received: 9 July 2024; Accepted: 9 August 2024
Published online: 21 August 2024

References

1. Larsen, H. D. *et al.* Preliminary report of an outbreak of SARS-CoV-2 in mink and mink farmers associated with community spread, Denmark, June to November 2020. *Euro Surveill.* **26**, 2100009. https://doi.org/10.2807/1560-7917.ES.2021.26.5.210009 (2021).
2. Rasmussen, T. B., Qvesel, A. G., Pedersen, A. G., Olesen, A. S., Fonager, J., Rasmussen, M., Sieber, R. N., Stegger, M., Artavia, F. F. C., Goedknegt, M. J. F, Thuesen, E. R., Lohse, L., Mortensen, S., Fomsgaard, A., Boklund, A. E., Bøtner, A. & Belsham, G. J. Emergence and spread of SARS-CoV-2 variants from farmed mink to humans and back during the epidemic in Denmark, June-November 2020. *BioRxiv* (2024). 2024.02.13.580053; https://doi.org/10.1101/2024.02.13.580053
3. Hammer, A. S. *et al.* SARS-CoV-2 Transmission between Mink (Neovison vison) and Humans, Denmark. *Emerg. Infect. Dis.* **27**, 547–551. https://doi.org/10.3201/eid2702.203794 (2021).
4. Fiedler, S. & Graw, M. Decomposition of buried corpses, with special reference to the formation of adipocere. *Naturwissenschaften* **90**, 291–300. https://doi.org/10.1007/s00114-003-0437-0 (2003).
5. Saukko, P. & Knight, B. *Knight´s Forensic Pathology* 4th edn. (CRC Press, 2016).
6. Pittner, S. *et al.* The applicability of forensic time since death estimation methods for buried bodies in advanced decomposition stages. *PLoS One* **15**, e0243395. https://doi.org/10.1371/journal.pone.0243395 (2020).
7. Hyde, E. R., Haarmann, D. P., Lynne, A. M., Bucheli, S. R. & Petrosino, J. F. The living dead: Bacterial community structure of a cadaver at the onset and end of the bloat stage of decomposition. *PLoS ONE* **8**, e77733. https://doi.org/10.1371/journal.pone.0077733 (2013).
8. Bahl, M. I. *et al.* The gastrointestinal tract of farmed mink (Neovison vison) maintains a diverse mucosa-associated microbiota following a 3-day fasting period. *Microbiol. Open* **6**(3), e00434. https://doi.org/10.1002/mbo3.434 (2017).
9. Schotsmans, M. J. E., Fletcher, J. N., Denton, J., Janaway, R. C. & Wilson, A. S. Long-term effects of hydrated lime and quicklime on the decay of human remains using pig cadavers as human body analogues: Field experiments. *Forensic Sci. Int.* **238**(141), 141. e1-141.e13 (2014).
10. Zhao, D. *et al.* Replication and virulence in pigs of the first African swine fever virus isolated in China. *Emerg. Microbes Infect.* **8**, 438–447. https://doi.org/10.1080/22221751.2019.1590128 (2019) (**PMID:30898043;PMCID:PMC6455124**).
11. Nguyen-Thi, T. *et al.* An assessment of the economic impacts of the 2019 African swine fever outbreaks in Vietnam. *Front. Vet. Sci.* **8**, 686038 (2021).
12. You, S. *et al.* African swine fever outbreaks in China led to gross domestic product and economic losses. *Nat. Food* **2**, 802–808 (2021).
13. Burrough, E. R. *et al.* Highly Pathogenic Avian Influenza A(H5N1) Clade 2.3.4.4b Virus Infection in Domestic Dairy Cattle and Cats, United States, 2024. *Emerg. Infect. Dis.* **29**, 30. https://doi.org/10.3201/eid3007.240508 (2024).
14. Plaza, P. I., Gamarra-Toledo, V., Euguí, J. R. & Lambertucci, S. A. Recent changes in patterns of mammal infection with highly pathogenic avian influenza A (H5N1) virus worldwide. *Emerg. Infect. Dis.* **30**, 444–452. https://doi.org/10.3201/eid3003.231098 (2024).
15. Rasmussen, T. B. *et al.* Infection, recovery and re-infection of farmed mink with SARS-CoV-2. *PLoS Pathogens* **17**, e1010068. https://doi.org/10.1371/journal.ppat.1010068 (2021).
16. Schotsmans, M. J. E. *et al.* Effects of hydrated lime and quicklime on the decay of buried human remains using pig carcasses as human body analogues. *Forensic Sci. Int.* **217**, 50–59 (2012).
17. Salihbegović, A. *et al.* Histological observations on adipocere in human remains buried for 21 years at the Tomašica grave-site in Bosnia and Herzegovina. *Bosn. J. of Basic Med. Sci.* **18**, 234–239. https://doi.org/10.17305/bjbms.2018.3343 (2018).
18. Aufderheide, A. C. *The Scientific Study of Mummies* 1st edn. (Cambridge University Press, 2013).
19. Volenec, F. J., Clark, G. M., Mani, M. M. & Humphrey, L. J. Burn wound biopsy bacterial quantitation: A statistical analysis. *Am. J Surg.* **138**, 695–697 (1979).
20. Rodríguez, W. C. & Bass, W. M. Decomposition of buried bodies and methods that may aid in their location. *J. Forensic Sci.* **30**, 836–852 (1985).
21. Dekeirsschieter, J. *et al.* Cadaveric volatile organic compounds released by decaying pig carcasses (*Sus domesticus* L.) in different biotopes. *Forensic Sci. Int.* **189**, 46–53. https://doi.org/10.1016/j.forsciint.2009.03.034f (2009).
22. Mahlknecht, J. Presence and persistence of SARS-CoV-2 in aquatic environments: A mini-review. *Curr. Opin. Environ. Sci. Health.* **29**, 100385 (2022).
23. Marzoli, F. *et al.* A systematic review of human coronaviruses survival on environmental surfaces. *Sci. Total. Environ.* **778**, 146191. https://doi.org/10.1016/j.scitotenv.2021.146191 (2021).
24. van Wyk, Y., Ubomba-Jaswa, E. & Dippenaar, M. A. Potential SARS-CoV-2 contamination of groundwater as a result of mass burial: A mini-review. *Sci. Total Environ.* **835**, 155473 (2022).
25. Wang, O.G., Scharling, M., Witthcen, K.B. & Kern-Hansen. C. 2001–2010 Dansk Design Reference Year Supplerende datasæt. Teknisk Rapport 13–18, Danmarks Meteorologiske Institut (2013). https://www.dmi.dk/fileadmin/user_upload/Rapporter/TR/2013/TR13-19.pdf
26. Cotmore, S. F. *et al.* The family Parvoviridae. *Arch. Virol.* **159**, 1239–1247. https://doi.org/10.1007/s00705-013-1914-1 (2014).
27. Eklund, C. M., Hadlow, W. J., Kennedy, R. C., Boyle, C. C. & Jackson, T. A. Aleutian disease of mink : Properties of the etiologic agent and the host responses. *J. Infect. Dis.* **118**, 510–526 (1968).
28. Hussain, I., Price, G. W. & Farid, A. H. Inactivation of aleutian mink disease virus through high temperature exposure in vitro and under field-based composting conditions. *Vet. Microbiol.* **173**, 50–58. https://doi.org/10.1016/j.vetmic.2014.07.014 (2014).
29. Prieto, A. *et al.* Application of real-time PCR to detect Aleutian Mink Disease Virus on environmental farm sources. *Vet. Microbiol.* **173**, 355–359. https://doi.org/10.1016/j.vetmic.2014.07.024 (2014).
30. Prieto, A. *et al.* Distribution of Aleutian mink disease virus contamination in the environment of infected mink farms. *Vet. Microbiol.* **204**, 59–63. https://doi.org/10.1016/j.vetmic.2017.04.013 (2017).
31. Hartby, C. M., Andersen, M. R., Kvisgaard, L. K., Chriél, M., Larsen, L. E., & Hjulsager, C. K. Pooling of faecal samples for quantitative virus diagnostics by real-time PCR. In A. Mäki-Tanila, J. Valaja, J. Mononen, T. Sironen, & O. Vapalahti (Eds.), *Proceedings of the XIth International Scientific Congress in Fur Animal Production* (pp. 27–30). Libris (2016). http://www.ifasanet.org/congress/2016/IFASA2016_Vol.40.pdf
32. Leong, E. *et al.* Design of mass burial sites for safe and dignified disposal of pandemic fatalities. *J. Environ. Geotech.* **8**, 208–216. https://doi.org/10.1680/jenge.20.00070 (2020).
33. Anon. 2021a. Rambøll Danmark A/S. Undersøgelse af området med minkgrave i Nr. Felding ved Holstebro (Version 03, Project No. 1100033606-017). Danish Ministry of Environment (2021). https://www.ft.dk/samling/20201/almdel/mof/spm/1320/svar/1787207/2403419.pdf
34. Anon. 2021b. Cowi A/S. Minkgrave Karup: Konceptuel hydrogeologisk model, risikovurdering, videre undersøgelsesforløb og forslag til afværgeforanstaltninger (Version 2.0, Project No. A218742-015-01). Danish Ministry of Environment (2021) https://www.ft.dk/samling/20201/almdel/mof/spm/1320/svar/1787207/2403423/index.html
35. Cassini, F., Scheutz, C., Skov, B. H., Mou, Z. & Kjeldsen, P. Mitigation of methane emissions in a pilot-scale biocover system at the AV Miljø Landfill, Denmark: 1. System design and gas distribution. *Waste Manag.* **63**, 213–225 (2017).

36. Scheutz, C., Cassini, F., De Schoenmaeker, J. & Kjeldsen, P. Mitigation of methane emissions in a pilot-scale biocover system at the AV Miljø Landfill, Denmark: 2. Methane oxidation. *Waste Manag.* **63**, 203–212 (2017).
37. Mønster, J., Samuelsson, J., Kjeldsen, P., Rella, C. W. & Scheutz, C. Quantifying methane emission from fugitive sources by combining tracer release and downwind measurements: A sensitivity analysis based on multiple field surveys. *Waste Manag.* **34**, 1416–1428 (2014).
38. Yoshida, H., Mønster, J. & Scheutz, C. Plant integrated measurement of methane and nitrous gas from a municipal wastewater treatment plant. *Water Res.* **61**, 108–118 (2014).
39. Scheutz, C., Samuelsson, J., Fredenslund, A. M. & Kjeldsen, P. Quantification of multiple methane emission sources at landfills using a double tracer technique. *Waste Manag.* **31**, 1009–1017 (2011).
40. Corman, V. M. *et al.* Detection of 2019 novel coronavirus (2019-nCoV) by real-time RT-PCR. *Euro. Surveill.* **25**, 2000045 (2020).
41. Quick, J. nCoV-2019 sequencing protocol V.1 (2020) https://doi.org/10.17504/protocols.io.bbmuik6w
42. Jørgensen, T.S. Sanger sequencing of a part of the SARS-CoV-2 spike protein (2021). https://doi.org/10.17504/protocols.io.bsbdnai6
43. Rasmussen, L. D., Karst, S.M., Richter, S.R., Midgley, S.E., Qvesel, A.G. & Franck, K.T. High throughput method for monitoring SARS-CoV-2 variants in wastewater by Nanopore sequencing. *Heliyon*, submitted.
44. Aksamentov, I., Roemer, C., Hodcroft, E. B. & Neher, R. A. Nextclade: Clade assignment, mutation calling and quality control for viral genomes. *J. Open Source Softw.* **6**, 3773. https://doi.org/10.21105/joss.03773 (2021).
45. Anon. a. Aerobic microorganisms. Determination in foods at 37 °C, 30 °C, 25 °C, 20 °C, 17/7 °C or 6.5 °C by the colony count method. NMKL-method 86, 5th edition (2013)
46. Anon. b. Sulphite-reducing Clostridia. Determination in Foods. NMKL-method 56, 5th edition (2015).
47. Alexi, N. *et al.* Potential of novel cadaverine biosensor technology to predict shelf life of chilled yellowfin tuna (*Thunnus albacares*). *Food Control* **119**, 107458 (2021).
48. Apprill, A., Mcnally, S., Parsons, R. & Weber, L. Minor revision to V4 region SSU rRNA 806R gene primer greatly increases detection of SAR11 bacterioplankton. *Aquat. Microb. Ecol.* **75**, 129–137 (2015).
49. Quast, C. *et al.* The SILVA ribosomal RNA gene database project: improved data processing and web-based tools. *Nucleic acids research*, **41**(D1), D590–D596.https://doi.org/10.1093/nar/gks1219 (2013).
50. Bolger, A. M., Lohse, M. & Usadel, B. Trimmomatic: A flexible trimmer for Illumina sequence data. *Bioinformatics* **30**, 2114–2120 (2014).
51. Magoč, T. & Salzberg, S. L. FLASH: Fast length adjustment of short reads to improve genome assemblies. *Bioinform.* **27**, 2957–2963 (2021).
52. Edgar, R. C. UPARSE: Highly accurate OTU sequences from microbial amplicon reads. *Nat. Methods* **10**, 996–998 (2013).
53. Caporaso, J. G. *et al.* QIIME allows analysis of high-throughput community sequencing data. *Nat. Methods* **7**, 335–336 (2010).
54. Quast, C. *et al.* The SILVA ribosomal RNA gene database project: Improved data processing and web-based tools. *Nucl. Acids Res.* **41**, D590–D596 (2013).
55. Albertsen, M., Karst, S. M., Ziegler, A. S., Kirkegaard, R. H. & Nielsen, P. H. Back to basics: The influence of DNA extraction and primer choice on phylogenetic analysis of activated sludge communities. *PLoS ONE* **10**, e0132783 (2015).
56. Chao, A. *et al.* Rarefaction and extrapolation with Hill numbers: A framework for sampling and estimation in species diversity studies. *Ecol. Monogr.* **84**, 45–67 (2014).
57. Hsieh, T. C., Ma, K. H. & Chao, A. iNEXT: An R package for rarefaction and extrapolation of species diversity (Hill numbers). *Methods Ecol. Evol.* **7**, 1451–1456 (2016).
58. De Vleeschauwer, A. *et al.* Comparative pathogenesis of an avian H5N2 and a swine H1N1 influenza virus in pigs. *PLoS One* **4**, 1–10. https://doi.org/10.1371/journal.pone.0006662 (2009).
59. Fouchier, R. A. M. *et al.* Detection of influenza a viruses from different species by PCR amplification of conserved sequences in the matrix gene. *J. Clin. Microbiol.* **38**, 4096–4101. https://doi.org/10.1128/jcm.38.11.4096-4101.2000 (2000).
60. Hagberg, E.E. Molecular diagnostics of Aleutian mink disease virus: Applied use of next genetration sequencing and phylogenetics. Ph.D. thesis, Technical University of Denmark (2017). link: https://orbit.dtu.dk/en/publications/molecular-diagnostics-of-aleutian-mink-disease-virus-applied-use-
61. Jensen, T. H., Christensen, L. S., Chriél, M., Uttenthal, Å. & Hammer, A. S. Implementation and validation of a sensitive PCR detection method in the eradication campaign against Aleutian mink disease virus. *J. Virol. Methods.* **171**, 81–85. https://doi.org/10.1016/j.jviromet.2010.10.004 (2011).
62. Ryt-Hansen, P. *et al.* Outbreak tracking of Aleutian mink disease virus (AMDV) using partial NS1 gene sequencing. *Virol. J.* **14**, 1–9. https://doi.org/10.1186/s12985-017-0786-5 (2017).
63. Kvisgaard, L. K. *et al.* A fast and robust method for full genome sequencing of porcine reproductive and respiratory syndrome virus (PRRSV) type 1 and type 2. *J. Virol. Methods.* **193**, 697–705. https://doi.org/10.1016/j.jviromet.2013.07.019 (2013).

Acknowledgements

We would like to thank staff from the Danish Veterinary and Food Administration and technical staff present on-site for helping at the disposal site. Special thanks are extended to the excavator operators for their contribution to the sampling of mink and soil. Additionally, we extend our appreciation to Peter Engelund Holm from the University of Copenhagen for his guidance on pH measurements, as well as to Cecilie Brandt Becker, Mette Marie Jensen, and Tenna Sturm Lind Andersen for their support with on-site sampling, sample transportation, and laboratory work. We are also thankful to Gitte Petersen and Vi Phuong Thi Nguyen for their assistance with microbiological and microbial community analyses.

Author contributions

K.K.M.T., J.J.L. and A.D. conceived the study, M.S.H. and H.E.J. analyzed pathological data, S.C. and P.K. analyzed gas emission data, K.K.M.T., J.J.L. and A.D. analyzed bacteriological data, L.K.K., F.B.H., L.L., T.B.R., L.D.R., A.E.B. and G.J.B. analyzed virology data, K.K. organized on-site samplings and retrieved specific information on burial sites, K.K.M.T., J.J.L. and A.D. wrote the article with comments by all authors.

Competing interests

The authors declare no competing interests.

Additional information

Supplementary Information The online version contains supplementary material available at https://doi.org/10.1038/s41598-024-69902-6.

Correspondence and requests for materials should be addressed to A.D.